Cross-correlation analysis empirically validated to quantify relative spatial distributions of fat and protein in two channel super-resolution microscopy images of dairy gels

Zachary J. Glover[a,c,d,*], Anne Højmark Bisgaard[a,c], Ulf Andersen[e], Megan J. Povey[d], Jonathan R. Brewer[b,c], Adam Cohen Simonsen[a,c]

[a]*Department of Physics, Chemistry and Pharmacy*
[b]*Department of Biochemistry and Molecular Biology*
[c]*University of Southern Denmark,Campusvej 55,5230 Odense, Denmark*
[d]*School of Food Science and Nutrition, University of Leeds,LS2 9JT, UK*
[e]*Arla Foods a.m.b.a, Agro Food Park 19, 8200 Aarhus, Denmark*

Abstract

The advent of super-resolution microscopy allows microstructures of foods to be explored in new depths, which when coupled with quantitative image analysis can provide a powerful analytical tool. Herein, a methodology is presented and applied to use a 2D spatial cross-correlation analysis to investigate the relative spatial arrangement of protein and fat in acid induced whole milk gels where the milk is either non-homogenised or has been homogenised at either 10 or 25 MPa. Two-channel images were taken using super-resolution Stimulated Emission Depletion (STED) microscopy and confocal microscopy. A term has been derived to extract the typical distance from the fat droplet surface and to the local maximum protein distribution.

*Corresponding author
Email addresses: `glover@sdu.dk` (Zachary J. Glover), `adam@memphys.sdu.dk` (Adam Cohen Simonsen)

The fat droplet size is determined through 2D spatial autocorrelation analysis. Methods of analysis are applied to global images and to region specific analysis focussing on individual fat droplets. Cross-correlation analysis has been empirically validated using generated images with precise spatial features corresponding to the features of interest in true microscopy images, over appropriate length scales. The protein microstructure, fat droplet size and distances between the fat droplets and protein network are characterised. There are significantly different distances between he fat droplets and protein network in the homogenised samples compared to the non-homogenised sample. The extracted separation distances are below the diffraction limit of light, highlighting the utility of super-resolution imaging.

1. Introduction

A foods microstructure contributes its macroscopic physical properties, behaviour during processing, final texture and mouthfeel, shelf-life stability and digestibility. The ability to be better able to characterise complex, multi-component microstructures will enable a greater fundamental understanding of how structures and interactions at the nano-scale affect properties on a macroscopic scale. Quantitative measurements of specific physical features have potential ramifications in the areas of linking structure to functionality, texture, tribology and nutrition and will allow for better product design, process optimisation and could directly feed into predictive screening models.

Developments in advanced microscopy techniques are opening avenues of imaging samples under different conditions and resolutions than has previously been possible. Super-resolution microscopy techniques are capable of imaging beyond the diffraction limit with minimally pertubative sample preparations, allowing imaging to take place at length scales of interest for complex colloidal systems, under conditions that are physiological, biologically and industrially relevant.

One of the advantages to confocal microscopy remains the fact that different components within a sample can be specifically labelled and imaged separately, (Michalski, Cariou, Michel, and Garnier, 2002). This tool has been used to image and understanding countless structures across many scientific disciplines. Given that STED microscopy is based on a confocal set up, this allows for confocal and STED imaging to be done in the same image in different channels, and ongoing developments are allowing for multiple coloured STED channels in a single image. This allows for certain structures

to be imaged with super-resolution alongside other specifically labelled components (Glover, Ersch, Andersen, Holmes, Povey, Brewer, and Simonsen, 2019).

An application for two-colour imaging in foods is the interaction between different proteins (Dubert-Ferrandon, Niranjan, and Grandison, [7]) or fat and proteins (Ong, Dagastine, Kentish, and Gras, 2010), which are ubiquitous to some extent in almost every foodstuff. In dairy systems milk is generally homogenised prior to product production, primarily to reduce the particle size of the fat droplets. Particle size reduction slows the rate at which they cream out of the milk, which could lead to phase separation or inhomogeneity in a final product. It is well understood that the process of reducing the fat droplet size, and increasing the fat surface area 10-fold, disrupts the native milk fat globule membrane (Sharma and Dalgleish, 1993). Following homogenisation there is insufficient milk fat globule membrane to cover all the newly exposed fat interface. Milk proteins, predominately casein molecules and small casein micelles bind to the oil-water interface to reduce the surface energy in the system through hydrophobic interactions (Lucey, Munro, and Singh, 1998) Cho, Lucey, and Singh, 1999), proteins from the whey fraction are found following heat treatment above 70 °C (Sharma and Dalgleish, 1993). The fat droplets now have protein molecules at their surface which are capable of participating in network formation and function as an 'active filler' (Van Vliet, 1988). Under subsequent destabilisation to induce casein micelle aggregation and gel formation these fat droplets now play an active role in network formation. With improved resolution of the protein network it is possible to image fat droplets embedded in a protein network

4

and asses the effects homogenisation has had on the degree of interaction between the fat and protein, which can be enhanced through quantitative image analysis.

Confocal imaging of dairy microstructures has been used widely (Lucey, Munro, and Singh, 1998; Lucey, Teo, Munro, and Singh, 1998; Auty, Twomey, Guinee, and Mulvihill, 2001) however, the conclusions drawn from the images are often through qualitative means (Ong, Dagastine, Kentish, and Gras, 2011). Michalski, Cariou, Michel, and Garnier (2002) conducted two colour confocal imaging on fat containing dairy microstructures and noted that image analysis would improve the utility of the images.

Quantitative analysis is required in order to extract the maximum amount of information from images. Establishing methods of image analysis that measure true physical features in an image allows these parameters to be directly related to different macroscopic properties in an way that might be more intuitive. Recently, it has been demonstrated that Stimulated Emission Depletion (STED) microscopy coupled with quantitative image analysis could be used to discriminate between different protein microstructures in dairy gels (Glover, Ersch, Andersen, Holmes, Povey, Brewer, and Simonsen, 2019). STED microscopy overcomes the diffraction limit through the use of a second laser that forms a torus shape and is overlayed with the excitation beam. The second laser is a depletion beam and forces fluorophores to emit photons at a higher wavelength. Emitted light at higher wavelength can be filtered out in the microscope enabling photons to be collected from a smaller area, thus reducing the pixel size Hell and Wichmann, 1994; Hell, 2003; Hell, Hell, 2008. The use of super-resolution microscopy, including

STED, offers the ability to image structures on smaller length scales than has been achieved previously without excessive sample preparations, fixing or drying but as of yet remains under-exploited in analysis food systems.

Correlation based image analysis has been used since 1993 (Petersen, Höddelius, Wiseman, Seger, and Magnusson), and has found broad application. Correlation based analysis has been used to analyse food systems since Ako, Durand, Nicolai, and Becu, (2009) demonstrated the use of fitting a stretched exponential to the radial decay of the autocorrelation image could be used to extract physical parameters. Autocorrelation based analysis has been applied various food structures from soy protein gels (Urbonaite, De Jongh, Van Der Linden, and Pouvreau, 2015) to mixed protein gels (Ainis, Ersch, Farinet, Yang, Glover, and Ipsen, 2019) and dairy systems (Balakrishnan, Nguyen, Schmitt, Nicolai, and Chassenieux, 2017). Recently the model used to fit to the radial decay of the autocorrelation image was modified to include a term that extracted a long order periodicity in the images corresponding to the inter-pore distance in the image. Fourier space analysis has been demonstrated to be appropriate for determination of the fractal dimension of the structures in an image (Glover et al., 2019). Other modes of correlation based image analysis, termed Image Correlation Spectroscopy (ICS) have been applied to probe a wide range of processes, many of which have biological applications (Petersen et al., 1993; Mir, Baggett, and Utzinger, 2012). There are several modifications of ICS which corresponds to the 2D spatial autocorrelation function, that look at changes over time, Temporal-ICS (TICS) (Kolin and Wiseman, Kolin and Wiseman, 2007), spatially between channels Image Cross-correlation Spectroscopy (ICCS)(Petersen, Wiseman,

et al., 1999) and spatio-temporal correlation (STICS) (Hebert, Costantino, and Wiseman, 2005). Spatial cross-correlation allows analysis to be performed between two different coloured microscopy channels, and can yield spatial information about both components. A method has been developed to be able to apply spatial cross-correlation analysis to images of dairy gels containing a protein network and distributed fat droplets.

In this paper a combination of super-resolution STED microscopy and confocal microscopy with quantitative 2D spatial autocorrelation and cross-correlation is presented and applied to two channel microscopy images of dairy gels containing protein and fat. The size of the fat droplets is extracted through autocorrelation analysis. The typical distance between a fat droplet interface to a maximum local distribution of protein is quantified through cross-correlation analysis. The method of cross-correlation analysis which involves a zero-lag mask removal of the fat channel from the protein channel has been empirically validated through the generation of artificial images, with precise spatial features. The image analysis methods have been applied to STED and confocal images of acid induced whole milk gels, where the milk was either non-homogenised or homogenised at either 10 or 25 MPa.

2. Materials & Methods

2.1. Sample preparation

Three fresh whole milk gel samples were produced from non-homogenised milk, single stage homogenised milk at 10 MPa or single stage homogenised milk at 25 MPa. Milk was locally purchased pasteurised and standardised to 3.5 % fat but not homogenised (Thise mejeri, Denmark). Milk was pooled

prior to the start of the sample preparation to ensure all samples came from the same batch. All milk was pre-heated to 60 °C to ensure the fat was in a liquid state before homogenisation. The non-homogenised milk was preheated to ensure uniformity of treatment. Milk was homogenised using a GEA Lab Homogenizer PandaPLUS 2000 (GEA, Dusseldorf, Germany) operating using a single stage at either 15 MPa or 25 MPa.

The fat in the milk was stained with Nile Red, to a final concentration of 2.5 μM in the milk. Stained samples were then left in the fridge overnight. Acid induced gels were produced by adding 0.25 g of Glucono-δ-Lactone (GDL)(Sigma-Aldrich, USA) to 10 ml of the pre-stained milk giving a final concentration of 2.5 % GDL in the milk. The 10 ml of milk with GDL was inverted by hand for 1 minute. 600 μl of milk was then sampled to which 3 μl of Atto 488 NHS-Ester (Atto-Tec GmbH, Siegen, Germany), dissolved in DMSO (99.9 % pure,Sigma-Aldrich) was added to give a final concentration of 510 μM in the milk. This volume was then transferred to a μ-Slide 8 Well chamber (ibidi, Germany), and incubated at 35 °C for 90 minutes. Milk samples were collected in triplicate, from each sample three gels were produced.

2.2. STED imaging

Imaging was performed using a Leica TSC SP8 STED microscope (Leica Gmbh, Mannheim, Germany). Samples were imaged after 90 minutes of incubation following GDL addition. Images were taken with two sequential channels, the first with excitation using an incident laser at 560 nm with detection between 570 and 700 nm, the second with excitation at 480 nm

and detection between 490 and 550 nm with STED depletion at 592nm. Both setups utilised a pulsed white light laser and gated hybrid detector (0.3 - 6 nm). The pixel size was optimised for STED acquisition at 29.9 nm, using 2.30 x digital zoom, producing images of 1688 x 1688 pixels equal to 50.44 μm^2 using a HCX PL AP 100X/1.40 OIL STED objective. Nine images were taken per gel, a total of 81 images per sample type. Images were taken > 5 μm above the glass interface to avoid boundary effects in the gel structure and fat droplets that may have spread on the glass surface. The suitability of Atto 488 NHS for STED imaging of dairy gels has been shown previously, including a negative control using CARS microscopy showing the presence of the dye does not affect the structures that form (Glover et al., 2019).

2.3. Cross-correlation, Autocorrelation and Fourier space image analysis

Image analysis of STED and CARS images was conducted with MATLAB R2018b. This image analysis generates an autocorrelation image of each channel and the cross-correlation image of both channels, as well as the power spectrum image. The images were pre-processed using Huygen's Software (Scientific Volume Imaging B.V., The Netherlands) and MATLAB. In which the fat channel images were background subtracted at a level corresponding to signal from the protein images. This was determined by drawing a line profile across the fat droplets and protein structures, where the two components could easily be distinguished based on their intensity values. This is clear in a 1D line profile, but it not something that can be clearly deduced based on the intensity histogram of the image. The protein channel was deconvoluted using automatically estimated background level.

Following this images were handled in MATLAB. For the cross-correlation

analysis and autocorrelation analysis of the fat channel the fat images were convert to binary images using the *'imbinarize'* function, based on a level determined from the *graythresh'* function as per Otsu's method. A smoothing filter of 2x2 pixels was applied to the STED protein images using the function *'wiener2'*. The area used is below the minimum size of any structures resolved and will not affect the detected features in the images.

Wherever there was intensity in the binarised fat channel, the corresponding pixels were set to zero in the protein channel image. This has been termed zero-lag mask removal. If any intensity remains in these pixels, the cross-correlation returns an autocorrelation type decay. In this cross-correlation analysis the spatial relationship between two components imaged in different channels is of interest relative to each other, and not how they directly lo-localise with each other in the original, zero-lag image. This pre-processing produces a cross-correlation curve with clear anti-correlation initially followed by a positive correlation peak. For the autocorrelation and power spectrum images of the STED protein channel the deconvoluted images were passed into the processing algorithm described below with no further pre-processing.

For all two colour microscopy images an autocorrelation image is calculated for each channel and the cross-correlation image is calculated from the pair of images. The 2D spatial autocorrelation definition is shown in equation 1

$$G(a,b) = \sum_{x=1}^{M} \sum_{y=1}^{N} I(x,y) \cdot I(x-a, y-b) \tag{1}$$

where $G(a, b)$ is the 2D spatial autocorrelation, of image, I, of MxN pixels. $I(x, y)$ is the intensity value in pixel (x, y) and a and b are the spatial lags from the corresponding x and y coordinates in I.

The 2D spatial cross-correlation definition is given in equation 2

$$C(a, b) = \sum_{x=1}^{M} \sum_{y=1}^{N} I_1(x, y) \cdot I_2(x - a, y - b) \tag{2}$$

where $C(a, b)$ is the 2D spatial cross-correlation, of images, I_1 and I_2, both of MxN pixels. $I_1(x, y)$ and $I_2(x, y)$ are the intensity values in pixels (x, y) in I_1 and I_2 and a and b are the spatial lags from the corresponding x and y coordinates in I_1 and I_2.

It is computationally more efficient to calculate the autocorrelation and cross-correlation functions from the inverse Fourier transform of the power spectrum image, descried by the Wiener-Khinchin theorem and shown in equations 3 and 4 for the autocorrelation and equations 5 and 6 for the cross-correlation (Robertson and George, 2012; Glover et al., 2019)

$$S(I) = \mathcal{F}[I(x, y)] \cdot \mathcal{F}^*[I(x, y)] \tag{3}$$

$$G(a, b) = \mathcal{F}^{-1}[S(I)] \tag{4}$$

where $S(I)$, is the power spectrum image, $\mathcal{F}(I(x,y)$ is the Fourier transform of image I, $G(a,b)$ is the 2D spatial autocorrelation, and $\mathcal{F}^{-1}$ is inverse Fourier transform. The power spectrum image is used in determining the fractal dimension of the protein network in the protein channel image (Glover et al., 2019). The cross-correlation image can be determined in the same way

$$S(I_1, I_2) = \mathcal{F}[I_1(x,y)] \cdot \mathcal{F}^*[I_2(x,y)] \tag{5}$$

$$C(a,b) = \mathcal{F}^{-1}[S(I_1, I_2)] \tag{6}$$

where $S(I_1, I_2)$ is the power spectrum image of images $I_1(x,y)$ and $I_2(x,y)$, $C(a,b)$ is the 2D spatial cross-correlation image.

Normalisation and mean subtraction removes intensity variations that may have arisen from the acquisition system and translates the correlation data to oscillate around zero, which is more intuitive to interpret in terms of positive and negative correlations. The normalised autocorrelation and cross-correlation images can be determined from the Fourier transform as shown in equations 7 and 8 respectively

$$g(a,b) = \frac{\mathcal{F}^{-1}[\mathcal{F}(I(x,y) - \langle I(x,y)\rangle) \cdot \mathcal{F}^*(I(x,y) - \langle I(x,y)\rangle)]}{\sigma(x,y)^2} \tag{7}$$

12

where $g(a,b)$ is the normalised autocorrelation image, $\sigma(x,y)$ is the standard deviation of the intensity values across the whole image, $\mathcal{F}^*(I(x,y))$ is the conjugate of the Fourier transform of the image and $\langle I(x,y) \rangle$ is the average intensity in the image (Robertson and George, 2012; Mir et al., 2012; Costantino, Comeau, Kolin, and Wiseman, 2005; Kolin and Wiseman, 2007; Glover et al., 2019).

The normalised cross-correlation equation is determined in the same way but with two input images

$$c(a,b) = \frac{\mathcal{F}^{-1}[\mathcal{F}(I_1(x,y) - \langle I_1(x,y) \rangle) \cdot \mathcal{F}^*(I_2(x,y) - \langle I_2(x,y) \rangle)]}{\sigma_1(x,y) \cdot \sigma_2(x,y)} \tag{8}$$

where $c(a,b)$ is the normalised cross-correlation image, $\sigma_1(x,y)$ is the standard deviation of the intensity values across Image 1, $I_1(x,y)$, and $\sigma_2(x,y)$ is the standard deviation of the intensity values across Image 2, $I_2(x,y)$. Angular brackets indicate the average intensity in the images, as above.

The radial distributions of the autocorrelation and cross-correlation images were calculated using the MATLAB *'acumarray'* function, as per Glover et al. (2019), which makes use of every pixel in the image. This method is suitable for isotropic systems, such as aggregated dairy system where there is no specific directionality or order to the structure. The radially averaged correlation plot is then normalised by dividing by the largest value to re-scale the correlation intensities from one, without affecting the distance data that is extracted.

To extract information from the radially averaged autocorrelation two different stretched exponential models have been utilised. The first, described by Ako et al. (2009) is applied to the microscopy images of the fat droplets, where equation 9 is used to extract the typical length of the fat droplet in the image. The second model, first described by Glover et al. (2019) is applied to the microscopy images of the protein network, where the stretched exponential decay extracts the typical length of the protein domains and a damped oscillatory function extracts the inter-pore distance in the protein network, shown in equation 10.

$$p(r) = C \cdot e^{-(\frac{r}{\xi_f})^\beta} \tag{9}$$

$$p(r) = C \cdot e^{-(\frac{r}{\xi_p})^\beta} \cdot \cos(\frac{2\pi(r - r_1)}{\lambda}) \tag{10}$$

The model shown in equations 9 and 10 are fit to the radial distribution of the autocorrelation images for the fat and protein channels respectively using the minimisation function *'fmincon'*, where r is the initial radial distance and r_1 is the displaced radial distance. In both equations 9 and 10 ξ represents the short order characteristic length scale with ξ_f for the fat image and ξ_p for the protein image. In equation 10 λ corresponds to the longer order characteristic length scale in the protein image.

In the radially averaged cross-correlation decay the peak maxima occurs

14

at a distance corresponding to the sum of the typical radius of a fat droplet and the typical distance to maximum protein intensity from a fat droplet. The decay length ξ extracted from the radially averaged autocorrelation decay of the fat channel image is used to determine the typical distance from a fat droplet to the maximum protein intensity by subtracting this value from the distance at which the peak maxima occurs in the cross-correlation curve. This principle is illustrated in figure 2.

The fractal dimension is determined from the radially averaged distribution of the power spectrum image, $S(I)$, defined in equation 3. The radial distribution is determined for the power spectrum image as described above and plotted on a log-log plot. The gradient of the linear part of the curve is determined as described by Glover et al. (2019). The gradient of the linear region β of the power spectrum decay is realted to the fractal dimension D_f through equation 11 (Super and Bovik, 1991; Marangoni, Acevedo, Maleky, Peyronel, Mazzanti, Quinn, Pink, et al., 2012; Glover et al., 2019).

$$D_f = 4 - (\beta/2) \tag{11}$$

From the analysis of each two color image, five parameters are extracted: ξ_f of the fat image, Λ_o the distance to protein maxima from a fat droplet, ξ_p of the protein image, λ and D_f. Data for samples of the same type were collated. Histograms were produced using a spline fit to represent the distribution of the data, where discrete points have been plotted to show the

15

mid point of the histogram bins so the raw data is shown alongside the fit.

Microscopy Images were processed with MATLAB and Fiji Image J for publication. Image analysis parameters extracted from the microscopy images were collated based on sample type. Histograms were produced an plotted as discrete points, and overlay of a kernel fit is shown with the raw histogram data. One-way ANOVA with post-hoc Tukey's honestly significant difference tests were performed using MATLAB.

2.4. Generated artificial images & image analysis validation

Artificial images were generated to represent fat droplets surrounded by a distributed phase in order to validate the interpretation of the cross-correlation data. In this case the distributed phase represents protein in the microscopy images, but this could represent any colloidal structures, whether it is a bicontinuous network as in the case of the protein gels, a stabilising interfacial layer extending from a surface or Pickering particles at an oil-water interface. This is not intended to be a physical simulation for the aggregation of a two component gel, but rather to provide images that contain precise spatial features, where a single parameter can be varied at one time. The parameters that can be modified in the generation of these images correspond to the output parameters that are extracted from the real microscopy images. The output parameters from the correlation analyses can then be plotted against the input parameters used to make the images. The two parameters of interest are the radius of the fat droplet and magnitude of the distributed phase, which is determined by varying the parameter Λ_i in equation 12.

$$Z(r) = (\frac{r - r'}{\Lambda_i^2}) \cdot e^{-(\frac{r - r'}{\Lambda_i})} \tag{12}$$

Where r is radial distance, r' is the radius of discs representing fat droplets in the simulated images. The offset of r' ensures that the distribution begins at the edge of the discs. Λ_i is a parameter to be varied. Herein, Λ_i, is the input term in equation 12 used in the artificial, generated images, and Λ_o represents the equivalent output parameter extracted from the real microscopy images through the cross-correlation analysis. Λ_o is equal to the typical distance from a fat droplet to the maximum protein intensity.

A specific image size was generated to correspond to the size of the microscopy images. Images were generated in two channels, one for the disc and one for the distributions. Random coordinates were generated to serve as the centre of the disc and distribution in each channel. These coordinates were screened to be at least 3x the distance of the disc radius from each other to ensure no overlap occurred. The discs and distributions were generated by dilation to either a fixed radius for the discs, or to a fixed size corresponding to the value of Λ_i in equation 12 taking into account the input radius of the disc r'. The generated images were produced with physical dimensions relevant for the microscopy images that were to be analysed with this method.

The artificial images were analysed with the autocorrelation and cross-correlation methods described above. The output of the disc radius plus Λ_i

was compared to the distance to the first maxima of the cross-correlation curve for when both the disc radius and Λ_i were varied. The output parameters of ξ_f and Λ_o were compared to the input parameters of the disc radius and Λ_i respectively. 21-step wise values for each input parameter were used, with 60 images being generated for each input values.

2.5. Angle dependent region of interest analysis

The cross-correlation analysis described above was applied to specific regions of interest (ROI) to quantify the protein distribution around a specific fat droplet. Fat droplets were identified in the fat channel microscopy images using the MATLAB function *'imfindcircles'*. The two channel image is radially cropped around the centre of one of the identified fat droplets. The size of the crop exceeds the size of the parameter Λ_o in the output of the cross-correlation analysis of the whole image, to ensure that the relevant information can be extracted from the ROI. The image is pre-processed in the same way as the cross-correlation analysis for the whole image, the fat image is binarised, wherever there is fat in the binarised images the intensity of the corresponding pixels in the protein image are set to zero. The cropped image is then split into radial segments corresponding to $\pi/8$. A circular ROI is used to prevent there being a different number of pixels in different segments. Each segment is then evaluated based on each pixels distance to the centre point. The intensities of pixels with the same distance to the centre are averaged, converting each segment into a 1D array. The cross-correlation analysis is then performed on each 1D array, yielding the radius of the fat droplet and Λ_o as a function of angle. The mean protein intensity is deter-

mined in each segment by summing the intensity of each pixel and dividing by the number of pixels. Radial plots of the fat droplet radius, Λ_o and mean protein intensity as a function of angle are then generated. This process is illustrated in figure 6.

3. Results & Discussion

3.1. Microscopy Images and Particle Size Distributions

Representative microscopy images of acid induced whole milk gels of the three samples under investigation are shown in figure 1a-c. The two channel images were acquired with confocal imaging for the fat droplets, shown in red and with STED imaging for the protein network shown in green. The optics of the acquisition system limit the STED effect to green dyes due to the fixed wavelength of the depletion laser. From the images it is possible to qualitatively observe that the images taken from samples where the milk had been homogenised (b-c) have more, smaller fat droplets compared to the non-homogenised samples (a). The particle size distribution of the three milk samples is shown in figure 1d. Homogenisation has a clear effect of reducing the particle size of the fat droplets in the milk. Static light scattering is sensitive to the proteins in the milk as well as the fat and are responsible for the peaks in the region of 10^{-2} to 10^{-1}. The population of fat droplets in the sample homogenised at 25 MPa are overlapping in size with the measured proteins and the two populations cannot be independently fit anymore. In this work it is not an issue that the smaller fat droplet population cannot be resolved from the proteins, as the particle size distributions are illustrating that there are clear differences between the non-homogenised sample

19

due to the homogenisation treatments. The particle size distribution of fat droplets in the images would not be the same as measured with the Mastersizer as when acquiring the images, very large fat droplets were excluded, firstly, because they were most often found sitting at the glass interface which was excluded to avoid boundary anomalies in the gel formation and droplet spreading. Secondly, the aim of this work was to develop a method based on cross-correlation of investigating how fat droplets became incorporated into a dairy gel network, and droplets of too large (>3 μm) were often not incorporated into the network as completely, or found as the slide interface. From a combination of autocorrelation and cross-correlation analysis it has been possible to quantify the typical radius of fat droplets in an image and determine the typical distance to the maximum protein intensity from the interface of the fat droplet.

3.2. Cross-correlation image analysis

Figure 2 illustrates the methodology behind the correlation analyses applied to the microscopy images, beginning with a two colour microscopy image in figure2a. This is then split into the two respective channels before these are further processed in figure 2b & c. Figure 2d-f show the generation of autocorrelation image from red, fat channel, $g - i$ shows the generation of the cross-correlation image from the red fat channel and the green protein channel. Both the auto and cross correlation images are radially symmetric, showing the microscopy images were isotropic, having no specific directionality to the distribution of fat or protein. For isotropic systems the correlation image can be radially averaged, the plots of which are shown in figure 2j for both the auto and cross correlation images. The model shown in equation

9 is used to fit to the autocorrelation decay and extract the typical radius of a fat droplet ξ_f in the image. The peak maxima in the radial decay of the cross-correlation curve corresponds to a distance equal to the sum of ξ_f and the typical distance to the maximum protein intensity from the edge of the fat droplet Λ_o. The distance from the fat droplet to the maximum protein intensity can then be isolated by subtracting the ξ_f from the peak maxima of the radial decay of the cross-correlation image. Validation of the interpretation of this parameters has been conducted using generated images.

3.3. Empirical validation with generated images

Figure 3 details the generation of images used in the cross correlation validation, including an example of a 1D profile from the centre of a disc through the distributed 'phase' around it (figure 3e). Each image generated contained discs of a specified size in a red channel (varied in figure 3a&b) and a radial distribution of a specific magnitude , around the disc, in a green channel(varied in figure 3 c & d). These images are not intended to fully represent the microscopy images of dairy gels, nor is this a physical simulation of the interaction between protein and fat in a dairy system. The method presented in figure 3 allows the production of images with precise spatial features in two channels. In order to be able to validate the output from the image analysis, images must be fed into it where the exact dimensions of each component are known, to observe whether this information is recovered in the output of the analysis. The physical parameters of interest were the size of the fat droplets and information about the spatial proximity of the protein to the fat droplets in the images. Controlling the size of the disc radius and the input parameter Λ_i into equation 12 has enables the validation of the

interpretation of the cross-correlation data.

An initial understanding of the cross-correlation radial decay where the green channel has undergone a zero-lag mask removal based on the structure in the red channel was established by varying the two input parameters available in the image generation, step wise, and observing different parameters in the radial decay curve. It was found that the distance to the first maxima correlated with the sum of the disc radius and Λ_i. Figure 4a shows correlation plots between the distance to the first maxima in the radial decay curve of the cross-correlation images as a function of the input parameters of the disc radius or Λ_i used in generation of the images. There is a strong linear correlation between the peak maxima and the sum of the disc radius and Λ_i when either the disc radius or Λ_i are varied.

There is more utility in knowing the size of the individual components than their sum, and it is known that the size of discs in an image can be extracted by fitting a stretched exponential model to the radial decay of the autocorrelation image. The model shown in equation 9 was fit to the radial decay of the autocorrelation image calculated for the red channel of every generated image. The fitting parameter ξ_f was extracted, corresponding to the decay length in the stretched exponential curve which was plotted against the input of the disc radius, shown in figure 4b. There is a strong linear correlation between the disc radius input into the generated images and the extracted output of ξ_f meaning that the information going into generating the red channel images is recovered in the image analysis.

Having established that the disc radius can be determined effectively, this could now be subtracted from the distance to the first maxima in the radial plot of the cross-correlation curve, which has been shown to correlate to the sum of the disc radius and Λ_i. When ξ_f is subtracted from the distance to the first maxima the distance from the fat droplet to the maximum intensity of the distributed phase in the green channel, Λ_o is left. Figure 4c shows there is a strong linear correlation between the input Λ_i and output Λ_o, indicating that the distance to the point of maximum intensity in the distributed phase from the disc can be recovered from the cross-correlation analysis.

The distribution of protein around fat droplets in the true microscopy images is not perfectly uniform as is the case in the generated images. The advantage to extracting the distance to the first maxima in the cross-correlation curve is that this corresponds to a physical length in the microscopy images, and is therefore unaffected by the amount, intensity or uniformity of the protein distribution around any fat droplets. If there were less protein, or sparsely distributed protein around the fat droplets this would be realised as a lower intensity in the normalised cross-correlation curve and not a shift in the peak position.

3.4. Cross-correlation and autocorrelation image analysis data

Having empirically validated the interpretation of the cross-correlation data it was now possible to apply it to true microscopy images of acid induced whole milk gels, following different pre-treatments. Figure 5 shows the

23

output from cross-correlation (figure 5a-b) and autocorrelation (figure 5c-e) image analysis on the three samples types under investigation.

From figure 5a it is possible to observe a difference in the distribution of the fat droplet size in the images between the non-homogenised sample and the two homogenised milk samples. The difference in fat droplet radius in the images is non-significant (p = <0.05) between the different samples. Whilst this may not be accurate for the fat droplet size distribution in the samples, this is due to the imaging procedure which will have been biased away from the very largest fat droplets, many of which appeared to be at the glass interface for the microscopy slide. The aim of this study is to be able to determine the size and relative spatial positioning of fat and protein in microscopy images and not whether a suitable sampling regime can be established for determining a particle size distribution in a sample.

Figure 5b shows the distributions of the distance to maximum protein intensity from the fat droplets, Λ_o, for the three samples. There is a significant difference (p = < 0.01) between the non-homogenised and both homogenised samples. As it has been shown that the size of the fat droplets in the images does not vary significantly, the changes in Λ_o are independent of the size of the fat droplets in the microscopy images and are due physical changes in the interaction between the fat and protein following homogenisation.

The image analysis parameters extracted from the autocorrelation analysis show there are some changes to the structure of the protein network due

24

to homogenisation. Figure 5c shows the typical length of the protein domains, ξ_p, in the gel network where there is a significant difference between the non-homogenised sample and the sample homogenised at 25 MPa (p = <0.05) and a trend towards significance between the samples homogenised at 10 and 25 MPa (p = <0.1) and no significant differences between the non-homogenised and homogenised at 10 MPa samples. There is a more notable effect on the inter-pore distance, λ in figure 5d, the difference between the non-homogenised sample and that homogenised at 10 MPa is significant (p = <0.05), between the non-homogenised and homogenised at 25 MPa trends towards significance (p = <0.1) and that between the two homogenised samples is highly significant (p = < 0.01). There are no significant changes in the distributions of the fractal dimension between any of the samples (p = < 0.05), figure 5e.

3.5. Region of interest cross-correlation analysis

The image analysis presented above extracts parameters based on the entire image, each image containing a distribution of fat droplet and protein aggregate sizes. This analysis is suitable for characterising and differentiating samples of different preparation and processing history. In some instances it may be of interest to look more specifically into smaller regions, in the context of this investigation to look at an individual fat droplet. The toolkit presented herein, can be applied to region of interest areas within the images to extract local information. The procedure to apply the cross-correlation method to region of interest areas is shown in figure 6. Figure 6a-d shows the pre-processing of the images from a cropped raw two colour image (a) to

25

the radially cropped binarised fat channel (b) the radially cropped protein image having undergone zero-lag mask removal of the fat image (c) and the overlay of treated protein and fat images (d). The image analysis within the region of interest is performed as a function of angle, figure 6e shows one angular segment of the protein image corresponding to an interval of $\pi/8$ meaning each image is split into 16 segments. The radius of the fat droplet is extracted and can be plotted on a radial plot to the same scale as the image, shown in figure 6f. Each segment is radially averaged to collapse it to a 1D array in which the cross-correlation analysis is performed, yielding Λ_o for each angle which is radially plotted in figure 6g. Λ_o shows the distance to the maximum protein intensity from the fat droplet as a function of angle. Finally the mean protein intensity within each segment is determined and plotted as a function of angle, figure 6h. The radial plot of mean protein intensity shows how much protein is distributed around the fat droplet, and shows the level of heterogeneity in this.

Region of interest specific analysis can be performed for multiple fat droplets. The effect of analysis multiple regions in this data set and averaging the data sets is of no benefit over the global cross-correlation analysis. However, by overlaying the radial plots of five different regions of interest it can be seen in figure 7 that the changes in fat droplet radius, distance to the maximal protein distribution and amount and anisotropy of the protein distribution can vary a lot. This methodology allows these parameters to be visualised in a quantitative way, providing a novel tool to be able to investigate the spatial relationship between two components in a complex colloidal

26

system.

The data presented above details how a 2D spatial cross-correlation can be applied to analyse two colour super-resolution microscopy images of the fat and protein in dairy gels. Appropriate pre-processing of the images has been performed using a zero-lag mask removal of the fat channel from the protein channel, enabling the analysis to probe the spatial relationship of the protein relative to the fat, from the interface of the fat droplet. The key output parameter Λ_o has been understood, and its interpretation validated through the use of precisely generated images, when paired with autocorrelation analysis of the fat channel to determine the typical size of fat droplet in the image, ξ_f.

Cross-correlation image analysis has been applied to three acid induced dairy gel samples produced from non-homogenised and homogenised (10 or 25 MPa) whole milk. From the autocorrelation analysis and model fitting (equation 9) of the fat channel the size of the typical size of the fat droplet in an image can be extracted effectively. The newly derived parameter Λ_o showed there was a significantly shorter distance to the maximal protein intensity from the fat droplet interface, in the homogenised samples compared to the non-homogenised sample. This can be explained by the fact that the fat droplets in native milk are stabilised by the Milk Fat Globule Membrane (MFGM)(Gallier, Gragson, Jimenez-Flores, and Everett, 2010), which contains a monolayer of surfactant molecules and an entire cellular phospholipid bilayer (Keenan, 2001). The MFGM keeps the native fat droplets stable, however with the increased shelf life possible with modern pasteurisation

27

it is preferable to avoid creaming of the fat through homogenisation. Homogenisation reduces the fat droplet size and vastly increases the surface area of the fat in the milk (Lucey et al., 1998). Following homogenisation there is not sufficient MFGM to stabilise the newly exposed fat droplet surface, and serum protein in the milk including casein molecules, small casein micelles and denatured whey proteins will bind the exposed fat surface, mediated through hydrophobic interactions thus reducing the surface energy in the system (Sharma and Dalgleish, 1993). When a homogenised system is then destabilised in a manner that will induce aggregation and gel formation, part of the surface of the fat droplets are effectively functionalised with material that can participate in the aggregation process (Van Vliet, 1988). Therefore, fat droplets milk proteins bound to their surface will seem to interact more closely with protein network, which is shown in figure 5b. Whilst the theory behind this is well known the change in this degree of interaction can now, not only be visualised with microscopy but quantified using the cross-correlation image analysis.

The data presented from the cross-correlation analysis is complementary to the data that can be extracted from autocorrelation and fourier space analysis of the protein channel image. The greatest degree of change in the system due to homogenisation would have been expected to relate to the decrease in fat droplet size and the proximity of the protein to the fat interface. However, subtle changes in the protein network are detected in both the typical length of the protein structures formed and the inter-pore distances in the gel network. The observed changes to the gel microstructure

may or may not impact strongly upon the final macroscopic properties of the gel / dairy product (Lucey et al., 1998; Cho et al., 1999). Relating the microstructure to macroscopic properties is not the focus of this study, but is it is noteworthy, given the range of products that will undergo some form of homogenisation, that homogenisation has a measurable effect on microstructure and further highlights how sensitive the toolkit of super-resolution imaging and this method of image analysis are to detecting changes in the structure of porous soft solid materials.

The benefit of super-resolution STED imaging can be seen in the data presented in figure 5b where the distances between the fat and protein are, for the smallest distance values extracted, below the diffraction limit of light (on the order of 250 nm). Whilst the fat channel is acquired with confocal imaging, the use of STED in the protein channel provides an added level of resolution required to determine the distance to the maximum protein intensity precisely. The use of image deconvolution for the STED images further improves the resolution in the images. This has had an effect on the fractal dimension values that have been obtained from analysis of these images. The deconvoluted images have diner structures to those presented in previous works, therefore a greater extent of the radial decay of the power spectrum image is occurring at larger values of q, corresponding to smaller structures, yielding fractal dimensions between 1 and 2 expected for planar structures captured in 2D. The interpretation of the fractal dimension can be interpreted as high values corresponding to a more jagged protein interface, leading to higher surface area (Smoczyński and Baranowska, 2014), although

29

the samples do not significantly vary due to the applied treatments in this study.

Region of interest specific analysis provides an avenue for specific, local analysis of two component systems, that will enable different questions to be asked of the system. Angle dependant analysis of the fat droplet size and surrounding protein network provides a novel method to probe specific regions of interest. The ability to be able to perform this type of image analysis globally or on localised regions of interest and extract information about the relative spatial relationship of two, or more, components has broad application in food and colloid science, surface chemistry and biophysics. Emulsion with adsorbed polymer layers, pickering stabilised emulsions, cell imaging with stained extra-cellular matrices and secretion of EPS from bacterial cultures could all be quantified with this type of image analysis. The quantification of such systems is therefore limited only by image acquisition. Advanced bioimaging is a field in which rapid advancements are being made, not only with the types, specificity and stability of available dyes, but in improved temporal and spatial resolutions and development of label free imaging modalities such as Coherent Anti-Stokes Raman Scattering (CARS) and Stimulated Raman Scattering(SRS) microscopies.

4. Conclusions

A methodology has been established to use 2D spatial cross-correlation analysis to determine the typical distance from fat droplet interface to the distributed protein phase. The fat droplet size is determined from 2D spa-

tial autocorrelation analysis. The analyses can be applied globally to images or to region specific areas to focus on individual fat droplets. The cross-correlation method has been validated using generated images with precise spatial features over a range of length scales relevant to true microscopy images. This analysis has been applied to images of whole milk gels and can significantly differentiate between samples that have been homogenised or not, even where there is not a significant difference in the size of the fat droplets in the images. Separation distances are determined below the diffraction limit of light, highlighting the utility of super-resolution microscopy in imaging multi-component, complex colloidal systems.

Acknowledgements

Competing interest statement

The authors have no competing interests.

References

[1] Ainis, W. N., Ersch, C., Farinet, C., Yang, Q., Glover, Z. J., Ipsen, R., 2019. Rheological and water holding alterations in mixed gels prepared

from whey proteins and rapeseed proteins. Food Hydrocolloids 87, 723–733.

[2] Ako, K., Durand, D., Nicolai, T., Becu, L., 2009. Quantitative analysis of confocal laser scanning microscopy images of heat-set globular protein gels. Food Hydrocolloids 23 (4), 1111–1119.

[3] Auty, M. A., Twomey, M., Guinee, T. P., Mulvihill, D. M., 2001. Development and application of confocal scanning laser microscopy methods for studying the distribution of fat and protein in selected dairy products. Journal of Dairy Research 68 (03), 417–427.

[4] Balakrishnan, G., Nguyen, B. T., Schmitt, C., Nicolai, T., Chassenieux, C., 2017. Heat-set emulsion gels of casein micelles in mixtures with whey protein isolate. Food Hydrocolloids 73, 213–221.

[5] Cho, Y., Lucey, J., Singh, H., 1999. Rheological properties of acid milk gels as affected by the nature of the fat globule surface material and heat treatment of milk. International Dairy Journal 9 (8), 537–545.

[6] Costantino, S., Comeau, J. W., Kolin, D. L., Wiseman, P. W., 2005. Accuracy and dynamic range of spatial image correlation and cross-correlation spectroscopy. Biophysical journal 89 (2), 1251–1260.

[7] Dubert-Ferrandon, A., Niranjan, K., Grandison, A. S., 2006. A novel technique for differentiation of proteins in the development of acid gel structure from control and heat treated milk using confocal scanning laser microscopy. Journal of dairy research 73 (4), 423–430.

[8] Gallier, S., Gragson, D., Jimenez-Flores, R., Everett, D., 2010. Using confocal laser scanning microscopy to probe the milk fat globule membrane and associated proteins. Journal of Agricultural and food Chemistry 58 (7), 4250–4257.

[9] Glover, Z. J., Ersch, C., Andersen, U., Holmes, M. J., Povey, M. J., Brewer, J. R., Simonsen, A. C., 2019. Super-resolution microscopy and empirically validated autocorrelation image analysis discriminates microstructures of dairy derived gels. Food Hydrocolloids 90, 62–71.

[10] Hebert, B., Costantino, S., Wiseman, P. W., 2005. Spatiotemporal image correlation spectroscopy (stics) theory, verification, and application to protein velocity mapping in living cho cells. Biophysical journal 88 (5), 3601–3614.

[11] Hell, S. W., 2003. Toward fluorescence nanoscopy. Nature biotechnology 21 (11), 1347.

[12] Hell, S. W., 2008. Microscopy and its focal switch. Nature methods 6 (1), 24.

[13] Hell, S. W., Wichmann, J., 1994. Breaking the diffraction resolution limit by stimulated emission: stimulated-emission-depletion fluorescence microscopy. Optics letters 19 (11), 780–782.

[14] Keenan, T. W., 2001. Historical perspective: milk lipid globules and their surrounding membrane: a brief history and perspectives for future research. Journal of mammary gland biology and neoplasia 6 (3), 365–371.

[15] Kolin, D. L., Wiseman, P. W., 2007. Advances in image correlation spectroscopy: measuring number densities, aggregation states, and dynamics of fluorescently labeled macromolecules in cells. Cell biochemistry and biophysics 49 (3), 141–164.

[16] Lucey, J., Munro, P., Singh, H., 1998. Rheological properties and microstructure of acid milk gels as affected by fat content and heat treatment. Journal of Food Science 63 (4), 660–664.

[17] Lucey, J. A., Teo, C. T., Munro, P. A., Singh, H., 1998. Microstructure, permeability and appearance of acid gels made from heated skim milk. Food Hydrocolloids 12 (2), 159–165.

[18] Marangoni, A. G., Acevedo, N., Maleky, F., Peyronel, F., Mazzanti, G., Quinn, B., Pink, D., et al., 2012. Structure and functionality of edible fats. Soft Matter 8 (5), 1275–1300.

[19] Michalski, M., Cariou, R., Michel, F., Garnier, C., 2002. Native vs. damaged milk fat globules: membrane properties affect the viscoelasticity of milk gels. Journal of Dairy Science 85 (10), 2451–2461.

[20] Mir, S. M., Baggett, B., Utzinger, U., 2012. The efficacy of image correlation spectroscopy for characterization of the extracellular matrix. Biomedical optics express 3 (2), 215–224.

[21] Ong, L., Dagastine, R., Kentish, S., Gras, S., 2010. The effect of milk processing on the microstructure of the milk fat globule and rennet induced gel observed using confocal laser scanning microscopy. Journal of food science 75 (3), E135–E145.

[22] Ong, L., Dagastine, R. R., Kentish, S. E., Gras, S. L., 2011. Microstructure of milk gel and cheese curd observed using cryo scanning electron microscopy and confocal microscopy. LWT-Food Science and Technology 44 (5), 1291–1302.

[23] Petersen, N., Wiseman, P., et al., 1999. Analysis of membrane protein cluster densities and sizes in situ by image correlation spectroscopy. Faraday discussions 111, 289–305.

[24] Petersen, N. O., Höddelius, P. L., Wiseman, P. W., Seger, O., Magnusson, K., 1993. Quantitation of membrane receptor distributions by image correlation spectroscopy: concept and application. Biophysical journal 65 (3), 1135–1146.

[25] Robertson, C., George, S. C., 2012. Theory and practical recommendations for autocorrelation-based image correlation spectroscopy. Journal of biomedical optics 17 (8), 080801.

[26] Sharma, S. K., Dalgleish, D. G., 1993. Interactions between milk serum proteins and synthetic fat globule membrane during heating of homogenized whole milk. Journal of Agricultural and Food Chemistry 41 (9), 1407–1412.

[27] Smoczyński, M., Baranowska, M., 2014. A fractal approach to microstructural changes during the storage of yoghurts prepared with starter cultures producing exopolysaccharides. Journal of texture studies 45 (2), 121–129.

[28] Super, B. J., Bovik, A. C., 1991. Localized measurement of image fractal dimension using gabor filters. Journal of visual communication and image representation 2 (2), 114–128.

[29] Urbonaite, V., De Jongh, H., Van Der Linden, E., Pouvreau, L., 2015. Water holding of soy protein gels is set by coarseness, modulated by calcium binding, rather than gel stiffness. Food hydrocolloids 46, 103–111.

[30] Van Vliet, T., 1988. Rheological properties of filled gels. influence of filler matrix interaction. Colloid and Polymer Science 266 (6), 518–524.
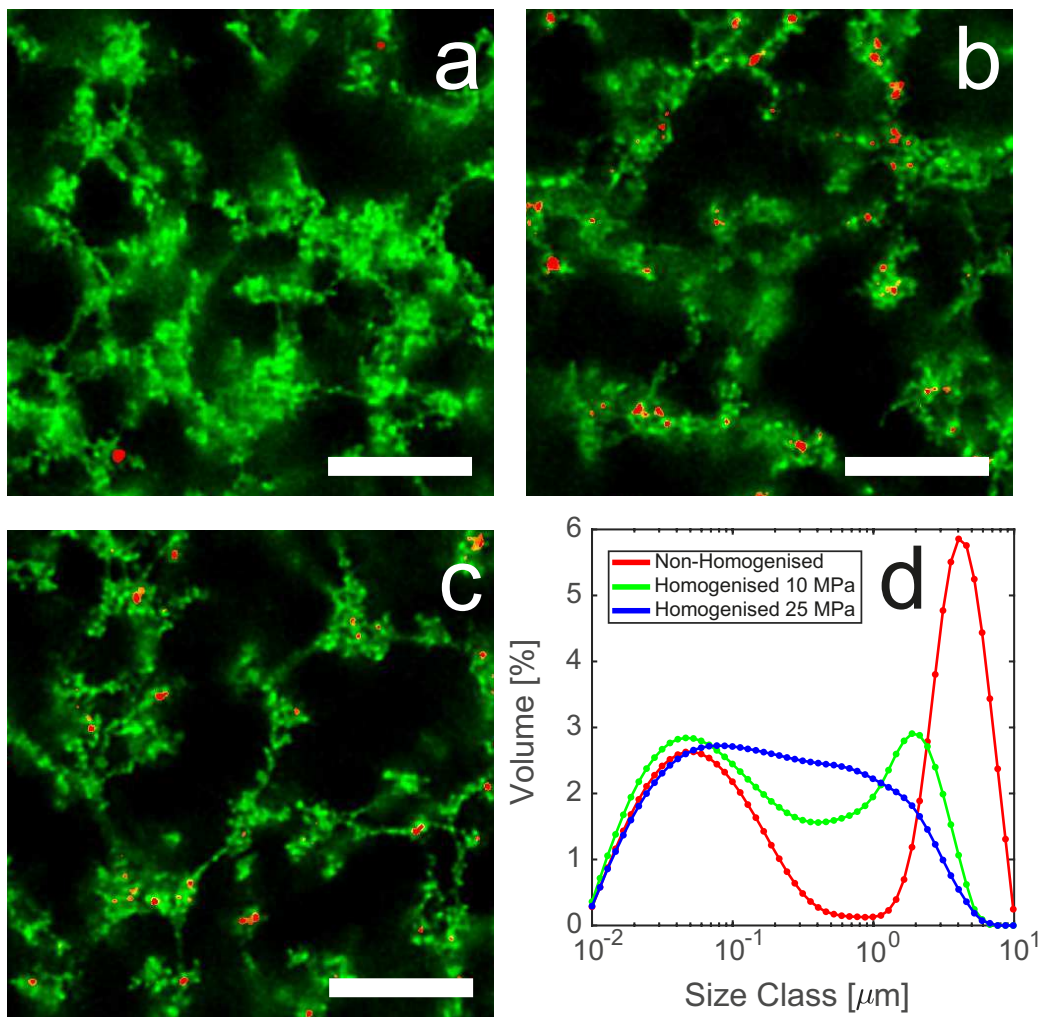
Figure 1: Representative STED and confocal microscopy images of the acid induced whole milk gel samples under investigation. Non-homogenised milk (a). Whole milk homogenised at 10 MPa (b). Whole milk homogenised at 25 MPa (c). All imaged after 90 minutes after acid addition at 35 °C. Scalebar 5 μm.
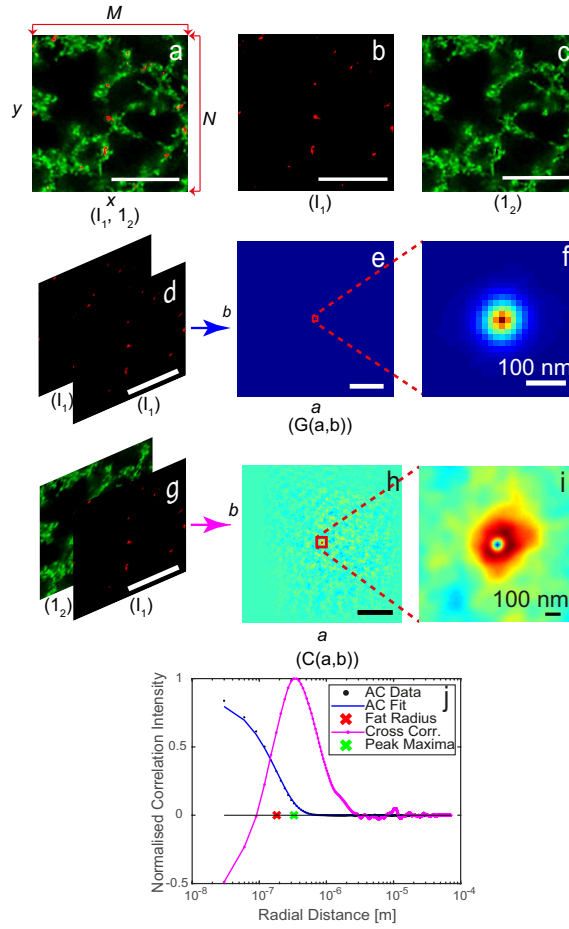
Figure 2: Workflow for the autocorrelation and cross-correlation analysis of two channel microscopy images. Two colour microscopy image of acid induced homogenised whole milk gel acquired with confocal microscopy for image I_1 with the fat shown in red and with STED for image I_2 where the protein is shown in green (a). Confocal image showing the fat channel in image a (b). Autocorrelation image calculated from the red confocal channel in a (c). Zoom in on the centre of the autocorrealtion image c (d). STED image showing the protein channel in image a (e). Cross-correlation image calculated from b and c (f). Zoom in on the centre of the cross-correlation image f (g). Plot of the normalised radially averaged autocorrelation decay from image c, shown in black points, to which a stretched exponential is fit(equation 9), shown in blue. The normalised radially averaged cross-correlation decay calculated from image f is shown in magenta. The fat droplet radius, ξ, (equation 9), is shown in red and the peak maxima of the cross-correlation curve is shown in green (h). Scalebar 5 μm, where not indicated on figure.
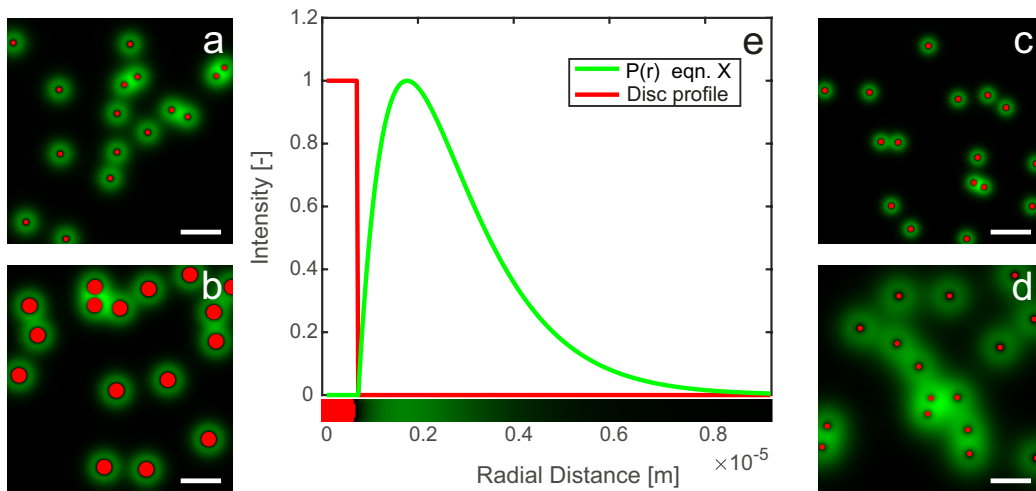
Figure 3: Illustration of the generation of two channel image each with precise spatial features or either a red disc representing a fat droplet or a green radial distribution based on equation 12 representing protein associated with a fat droplet. Generated images are used to validate the interpretation of the cross-correlation analysis. Randomly distributed red discs of varying radius with fixed green distribution (a,b). Randomly distributed red discs of fixed size, with varying size of green distribution (b,c). Plot to illustrate the 1D profile of the generated images showing a radial profile from the centre of a red disc. The green distribution is determined from equation 12, a radial slice of a generated image is overlayed below the x-axis to illustrate how the plot relates to the actual structures in the images (e). Scalebar 10 μm.
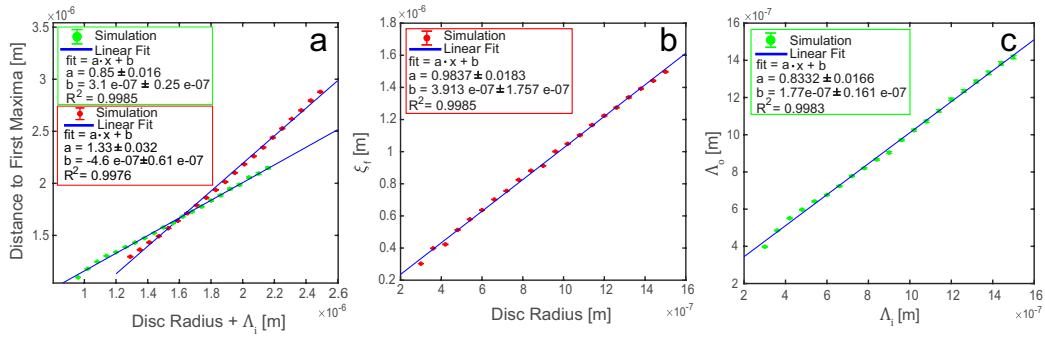
Figure 4: Correlation plots of the output parameters from the cross-correlation analysis against the input parameters used to to generate the artificial images shown in figure 3. Correlation plots of the disc radius plus the value of Λ used in equation 12 with the peak maxima from the plot of the normalised radially averaged cross-correlation plot, when the disc radius is varied, show in red, or when Λ is varied, shown in green (a). Correaltion plot of the disc radius with the parameter ξ extracted from the autocorrelation analysis of the red channel image (b). Correlation plot of the input parameter Λ used to generate the profile in equation 12 with the distance to the distribution maxima, determined from the maximum position in the cross-correlation curve, minus the value of ξ, determined from the autocorrelation analysis of the red channel image (c). Each data-point in the correlation plots (a,b,c) is an average of 60 runs with errorbars as standard error of the mean.
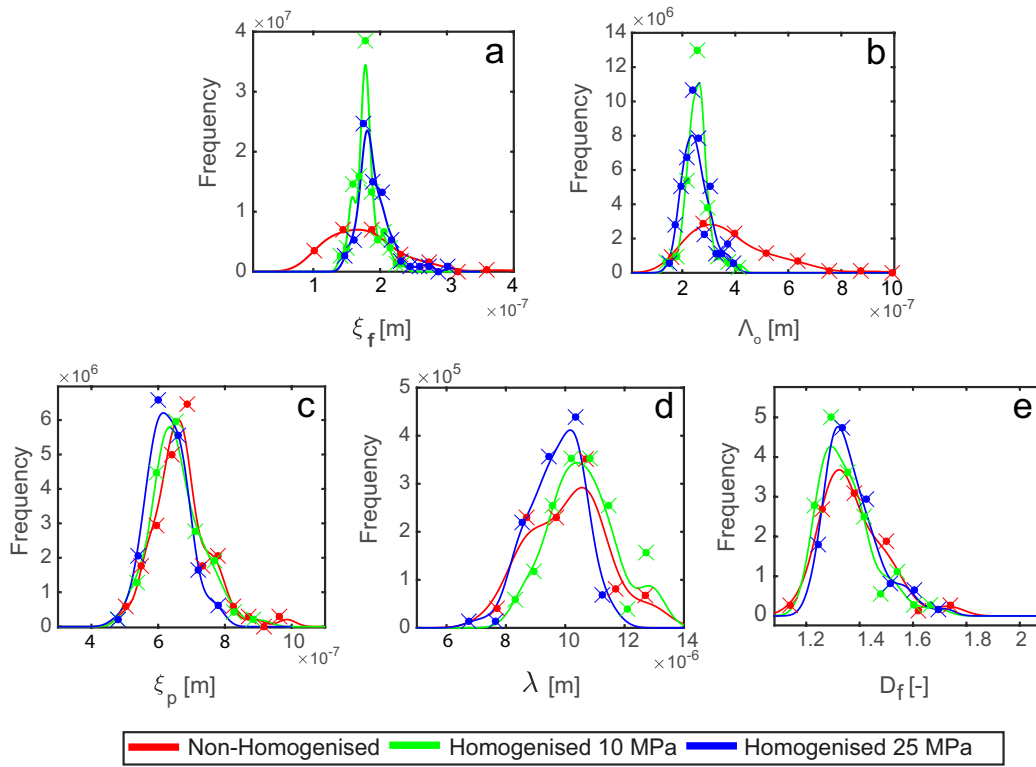
Figure 5: Output from cross-correlation and autocorrealtion image analysis of acid induced whole milk gels from non-homogenised and homogenised (10 or 25 MPa) milk. ξ of fat (a). Distance to Protein Maxima (b). ξ of protein network (c). λ of protein network (d). D_f from protein network (e).
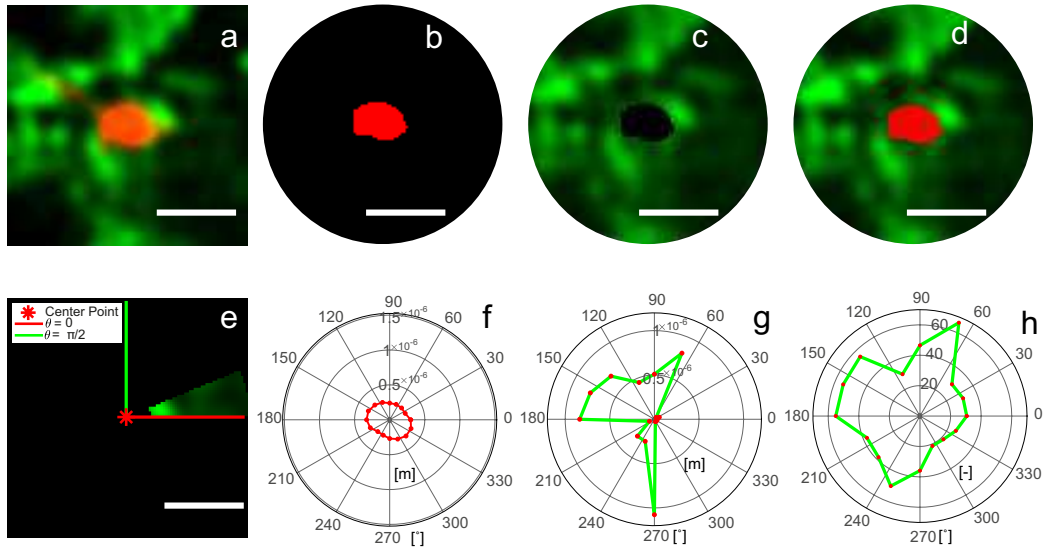
Figure 6: Workflow for spatial cross-correlation analysis of two colour microscopy images within a defined region of interest with angle dependent output. Cropped region of interest of two colour microscopy image, fat shown in red, protein in green (a). Binarised and cropped image of red channel shown in a (b). Circular crop of green channel in image a, pixel values have been set to zero wherever there is intensity in the corresponding red channel b (c). Overlay of b and c (d). Example of how the protein channel is segmented for angle dependent analysis, showing one segment of the image shown in c corresponding to $\pi/8$ (e). Radial plot of the radius of the fat droplet in b, as a function of angle (f). Radial plot of the angle dependent distance to protein maxima in c, measured from the boundary between the fat and protein (g). Radial plot of the mean protein intensity in c as a function of angle (h). Scalebar 1 μm.
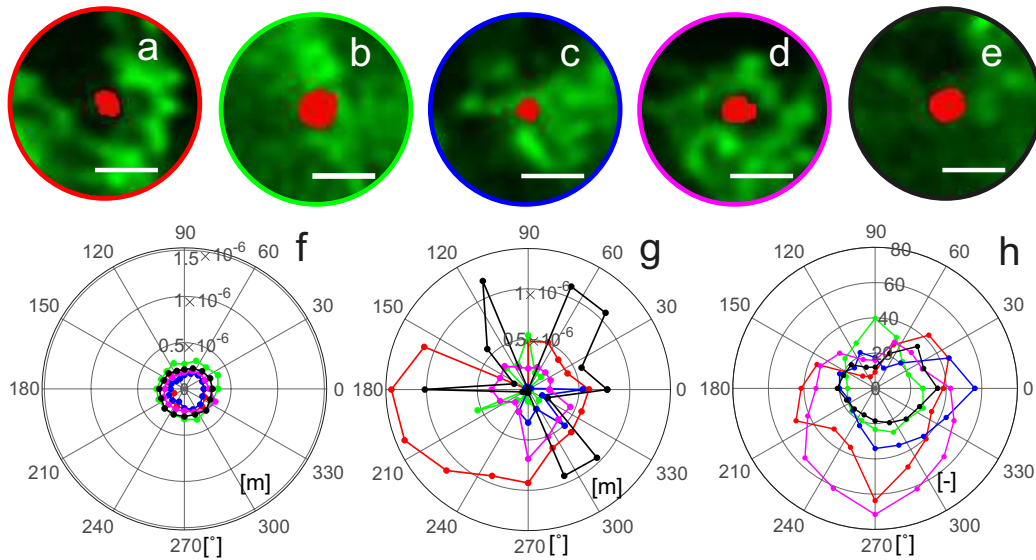
Figure 7: Angle dependent heterogeneity of distance to protein maxima and mean protein intensity around a specific fat droplets in two colour microscopy images of acid induced whole milk gels. Radially cropped two colour confocal and STED images of fat droplets, shown in red, and protein, shown in green (a-e). Radial plot of the fat droplet radii from $a - e$ (f). Radial plot of the distance to protein maxima determined from angle dependent cross-correlation analysis as shown in 6 (g). Radial plot of the mean protein intensity around a fat droplet as a function of angle (h). The boarder colours in $a - e$ correspond to the plot colours in $f - h$. Scalebar 1 μm.